

UNIVERSIDAD DE CONCEPCIÓN



CENTRO DE INVESTIGACIÓN EN  
INGENIERÍA MATEMÁTICA (CI<sup>2</sup>MA)



An efficient third-order WENO scheme with unconditionally  
optimal accuracy

ANTONIO BAEZA, RAIMUND BÜRGER,  
PEP MULET, DAVID ZORÍO

PREPRINT 2019-19

SERIE DE PRE-PUBLICACIONES



# AN EFFICIENT THIRD-ORDER WENO SCHEME WITH UNCONDITIONALLY OPTIMAL ACCURACY

ANTONIO BAEZA\*, RAIMUND BÜRGER†, PEP MULET‡, AND DAVID ZORÍO§

**Abstract.** A novel third-order Weighted Essentially Non-Oscillatory (WENO) scheme, attaining unconditionally third order accuracy when the data is smooth enough, even in presence of critical points, and second order accuracy if a discontinuity crosses the data, is presented. The key to attribute these properties to this scheme is the inclusion of an additional node in the data stencil, which is only used in the computation of the weights measuring the smoothness. The accuracy properties of this scheme are proven in detail and several numerical experiments are presented, which show that this scheme is more efficient in terms of the CPU cost/error ratio than its traditional third-order counterparts as well as several higher-order WENO schemes that are found in the literature.

**Keywords:** Finite-difference schemes, third order WENO reconstructions, optimal accuracy, efficiency

**Mathematics subject classifications (2000):** 65M06

## 1. Introduction.

**1.1. Scope.** Weighted Essentially Non-Oscillatory (WENO) schemes have become very popular, especially in the context of hyperbolic conservation laws, since they were proposed in [11] and later improved in [9]. One of the most used schemes in the literature is the fifth-order WENO scheme, which in general attains high efficiency in terms of the ratio CPU cost/error on weak solutions of hyperbolic conservation laws.

Third-order schemes have been usually dropped from usage due to a worse performance in terms of the aforementioned efficiency ratio, since, although they are much faster than the higher-order alternatives, their error in problems with weak solutions is also much higher, so that the ratio CPU cost/error is, in general, worse than those obtained by fifth-order WENO schemes.

In this paper we inspect the causes of the misperformance involving the traditional third-order WENO schemes through an analysis of their accuracy near critical points. We propose several solutions to this issue, by first proving that it is impossible to prevent accuracy loss near critical points in stencils with only three points, but it is possible to do so with stencils of at least four points. Ultimately the goal is to present a genuine third-order scheme that is competitive with the most commonly used fifth-order schemes for problems with weak solutions.

**1.2. Related work.** To put this work into the proper perspective, we mention that several previous attempts have been made in order to solve the issue involving the accuracy loss near critical points. For instance, in [19], the authors propose a novel smoothness measure based on introducing an additional exponent in the weight formula proposed in [20], associated to WENO-N3 schemes. However, although this measure solves the issue of the accuracy loss near critical points, in this case the resulting weights end up depending on the scaling of the data due to the additional

---

\*<sup>A</sup>Departament de Matemàtiques, Universitat de València, Av. Vicent Andrés Estellés, E-46100 Burjassot, Spain. E-Mail: [antonio.baeza@uv.es](mailto:antonio.baeza@uv.es)

†<sup>B</sup>CI<sup>2</sup>MA and Departamento de Ingeniería Matemática, Universidad de Concepción, Casilla 160-C, Concepción, Chile. E-Mail: [rburger@ing-mat.udec.cl](mailto:rburger@ing-mat.udec.cl)

‡<sup>C</sup>Departament de Matemàtiques, Universitat de València, Av. Vicent Andrés Estellés, E-46100 Burjassot, Spain. E-Mail: [pep.mulet@uv.es](mailto:pep.mulet@uv.es)

§<sup>D</sup>CI<sup>2</sup>MA, Universidad de Concepción, Casilla 160-C, Concepción, Chile. E-Mail: [dzorio@ci2ma.udec.cl](mailto:dzorio@ci2ma.udec.cl)

exponent. Other works improving this idea have been also done, but the issue of the weights depending on the scaling of the data in the weight design still remains; see for instance [6, 7, 21].

There are also many other works tackling the issue by tuning the parameter  $\varepsilon$  appearing in the weight design, which was initially conceived to be a small quantity used to avoid divisions by zero near constant data, but that was proven later to be crucial to avoid the accuracy loss near critical points if it was scaled properly, see for instance [1]. There are some recent works which tackle this issue in third-order schemes and limiters, for instance [14, 15].

We will show in this work that it is not possible to build a third-order reconstruction with a stencil of three points satisfying at once the following properties:

- Detection of discontinuities in the data.
- Detection of critical points in the data.
- Independence of non-linear weights of the scaling of the data (the issue appearing in [19]).
- Unnecessity of tuning/scaling  $\varepsilon$  (in contrast to the proposals in, e.g., [1, 15]).

And, once exposed, we will propose a novel WENO3 reconstruction method satisfying at once the aforementioned properties, by using stencils with an additional point, namely, a stencil containing a total of four points. This does not represent an increase of the stencil used to compute the numerical divergence in a semi-discrete scheme, as proven in 3.2.

**1.3. Outline of the paper.** This paper is divided as follows: Section 2 starts with some preliminaries and definitions that will be used along this paper, followed by a motivation in Subsection 2.3 in which we prove through a counterexample that a third-order WENO scheme cannot attain the optimal accuracy near critical points if a stencil of only three points is used, but that it is possible to attain the optimal accuracy even near critical points if an additional point is added. The proposed scheme, attaining unconditionally third order, is presented in Subsection 2.4. In Section 3 the key to use this reconstruction strategy in the context of third-order schemes for hyperbolic conservation laws without increasing the computational domain is shown. Section 4 stands for several validation numerical experiments in which our proposed schemes are compared against the most commonly used fifth-order scheme in terms of efficiency; finally, in Section 5 some conclusions are drawn.

## 2. Optimal third-order scheme.

### 2.1. Preliminaries.

DEFINITION 2.1. Assume that  $\alpha \in \mathbb{Z}$ . we write  $f(h) = \mathcal{O}(h^\alpha)$  to denote that  $\limsup_{h \rightarrow 0} |f(h)/h^\alpha| < \infty$ , and  $f(h) = \bar{\mathcal{O}}(h^\alpha)$  if  $f(h) = \mathcal{O}(h^\alpha)$  and in addition  $\liminf_{h \rightarrow 0} |f(h)/h^\alpha| > 0$ .

Since, for positive  $f, g$ ,

$$\begin{aligned} \limsup_{h \rightarrow 0} f(h)g(h) &\leq \limsup_{h \rightarrow 0} f(h) \limsup_{h \rightarrow 0} g(h) \\ \liminf_{h \rightarrow 0} f(h)g(h) &\geq \liminf_{h \rightarrow 0} f(h) \liminf_{h \rightarrow 0} g(h) \end{aligned}$$

it follows that  $\mathcal{O}(h^\alpha)\mathcal{O}(h^\beta) = \mathcal{O}(h^{\alpha+\beta})$  and  $\bar{\mathcal{O}}(h^\alpha)\bar{\mathcal{O}}(h^\beta) = \bar{\mathcal{O}}(h^{\alpha+\beta})$ .

**2.2. Third-order WENO reconstructions.** For the sake of exposition, we briefly describe two classical third-order WENO approaches. The first is the third-order WENO method defined by the Jiang-Shu approach [9] (henceforth, JS-WENO3)

and the second is the third-order WENO method through the Yamaleev-Carpenter approach [22,23] (henceforth, YC-WENO3). Since they have many parts in common, we will describe both approaches altogether while pointing out the key differences when necessary.

The input for both cases is an equally spaced three-point stencil  $(x_{-1}, x_0, x_1)$ ,  $x_i - x_{i-1} = h > 0$ ,  $i \in \{0, 1\}$ , associated with values  $(f_{-1}, f_0, f_1)$ , where either  $f_i = f(x_i)$  (reconstructions from point values) or

$$f_i = \frac{1}{h} \int_{x_{i-1/2}}^{x_{i+1/2}} f(x) dx$$

(reconstructions from cell averages). Here  $x_{i+1/2} = (x_i + x_{i+1})/2$ , and  $\varepsilon > 0$  is a parameter which is intended to be merely a small positive quantity avoiding divisions by zero. We assume that a right-biased reconstruction is sought, so the output is intended to be an approximation of  $f(x_{1/2})$ . The smoothness indicators are then defined as follows:

$$(2.1) \quad I_0 = (f_0 - f_{-1})^2, \quad I_1 = (f_1 - f_0)^2.$$

as well as the corresponding interpolating polynomials associated to each 2-point substencil:

$$(2.2) \quad p_0(x_{1/2}) = -\frac{1}{2}f_{-1} + \frac{3}{2}f_0, \quad p_1(x_{1/2}) = \frac{1}{2}f_0 + \frac{1}{2}f_1.$$

Now, in each case we define

$$\alpha_i = \begin{cases} \frac{c_i}{I_i + \varepsilon} & \text{for JS-WENO methods,} \\ c_i \left( 1 + \frac{\sigma}{I_i + \varepsilon} \right) & \text{for YC-WENO methods,} \end{cases}$$

where  $\sigma = (f_1 - 2f_0 + f_{-1})^2$  and

$$(2.3) \quad (c_0, c_1) = \begin{cases} (1/4, 3/4) & \text{in case of reconstruction from point values,} \\ (1/3, 2/3) & \text{in case of reconstructions from cell averages.} \end{cases}$$

Then, the non-linear weights are computed as

$$\omega_i = \frac{\alpha_i}{\alpha_0 + \alpha_1}, \quad i = 0, 1,$$

and the WENO reconstruction is finally given by

$$p_2(x_{1/2}) = \omega_0 p_0(x_{1/2}) + \omega_1 p_1(x_{1/2}).$$

**2.3. On the accuracy loss of third-order WENO schemes.** In the sequel we will abuse language by referring to the values of a function on a stencil as the stencil itself.

The following example shows that if a grid  $x_{i,h} = z + (c + i)h$ ,  $i \in \{-1, 0, 1\}$ , samples a function  $f \in \mathcal{C}^2$  such that  $f'(z) = 0$  and  $f''(z) \neq 0$ , then there are cases in which, ignoring the scaling of the stencil  $(f_{-1,h}, f_{0,h}, f_{1,h})$ , with  $f_{i,h} = f(x_{i,h})$ , the reconstruction obtained from that stencil for any given  $h$  is the same as if the

function had a discontinuity in it, and thus there cannot be scaling-independent and dimensionless parameters constructed from the data capable of distinguishing one case from the other.

Let us consider, for instance, an extreme case by considering  $f : \mathbb{R} \rightarrow \mathbb{R}$  given by  $f(x) = 4x^2$ , which satisfies  $f'(0) = 0$  and  $f''(0) = 8 \neq 0$ , and the grid  $x_{i,h} = (\frac{1}{2} + i)h$ ,  $i \in \{-1, 0, 1\}$ . Then the stencil  $F_h = (f_{-1,h}, f_{0,h}, f_{1,h})$ , with  $f_{i,h} = f(x_{i,h})$ , is given by  $F_h = (h^2, h^2, 9h^2)$ .

On the other hand, we define  $g : \mathbb{R} \rightarrow \mathbb{R}$  given by  $g(x) = 1$  if  $x < 0$  and  $g(x) = 9$  if  $x \geq 0$ , with the same grid as above. Then the stencil  $G_h = (g_{-1,h}, g_{0,h}, g_{1,h})$  is given by  $G_h = (1, 1, 9)$ .

Now, the relationship  $F_h = h^2 G_h$  holds for all  $h > 0$ ; that is, both stencils are, for fixed  $h$ , a scaled version of the same stencil. Therefore, any procedure to analyze smoothness agnostic about the scaling of the data will fail at distinguishing the first case, consisting of smooth data, from the second one, based on data taken from both sides of a discontinuity. Therefore, either such procedure, depending on its construction, will detect asymptotically both cases as smooth data, or will interpret both as discontinuous data, being in both cases wrong (giving either false negatives or false positives). The traditional third-order WENO schemes, belong to the latter group, in which the detection of discontinuities is prioritized against the detection of critical points, and thus the latter ones are interpreted incorrectly as discontinuities.

**2.4. Unconditionally optimal third-order scheme with an additional node.** We next present a novel scheme with essentially non-oscillatory properties which attains unconditionally the optimal order of accuracy.

Let  $S := (f_{-1}, f_0, f_1)$  be a stencil from a uniform grid,  $f_i = f(x_i)$ ,  $i \in \{-1, 0, 1\}$ ,  $x_i = z + (c + i)h$ ,  $i \in \{-1, 0, 1\}$ , and  $\tilde{S} := S \cup \{f_2\} = (f_{-1}, f_0, f_1, f_2)$  the extended stencil. Let us assume that one wants to perform a (right-biased with respect to  $S$ ) reconstruction at  $x_{1/2} := (x_0 + x_1)/2$  accounting for discontinuities. Then, both for reconstructions from point values and from cell averages, we define the following items:

In the first place, we define the corresponding interpolating polynomials associated to the substencils  $S_0 = (f_{-1}, f_0)$  and  $S_1 = (f_0, f_1)$  evaluated at  $x_{1/2}$ , which are given by (2.2). Their associated Jiang-Shu smoothness indicators [9] are thus given by (2.1). One of the keys here is to define also an additional smoothness indicator, in which the additional node is used:

$$(2.4) \quad I_2 = (f_2 - f_1)^2.$$

Now, given a small quantity  $\varepsilon > 0$ , we define the following weights:

$$(2.5) \quad \tilde{\omega}_0 := \frac{I_1 + \varepsilon}{I_0 + I_1 + 2\varepsilon}, \quad \tilde{\omega}_1 := \frac{I_0 + \varepsilon}{I_0 + I_1 + 2\varepsilon} = 1 - \tilde{\omega}_0.$$

We introduce now the corrector weight, given by

$$(2.6) \quad \omega = \frac{J}{J + \tau + \varepsilon}, \quad \text{with } J = I_0(I_1 + I_2) + (I_0 + I_1)I_2,$$

which clearly satisfies  $0 \leq \omega \leq 1$ , and  $\tau$  the product of the square of the undivided difference associated to the extended stencil  $\tilde{S}$  with the sum of the smoothness indicators:

$$(2.7) \quad \tau := dI, \quad d := (-f_{-1} + 3f_0 - 3f_1 + f_2)^2, \quad I := I_0 + I_1 + I_2.$$

We then define the corrected weights as

$$(2.8) \quad \omega_0 := \omega c_0 + (1 - \omega)\tilde{\omega}_0, \quad \omega_1 := \omega c_1 + (1 - \omega)\tilde{\omega}_1,$$

where  $c_0$  and  $c_1$  are specified in (2.3). Finally, the reconstruction result is given by

$$(2.9) \quad p(x_{1/2}) = \omega_0 p_0(x_{1/2}) + \omega_1 p_1(x_{1/2}).$$

The key to analyze the accuracy of our proposed scheme is to first study the accuracy of the corrector weight  $\omega$ .

**DEFINITION 1.** *We say that a function  $f$  has a critical point of order  $k \geq 0$  at  $x$  if  $f^{(l)}(x) = 0$  for  $l = 1, \dots, k$  and  $f^{(k+1)}(x) \neq 0$ .*

**PROPOSITION 2.** *If  $f$  has a critical point at  $z$  of order  $k$ ,  $k \in \{0, 1\}$ , there holds*

$$\omega = \begin{cases} 1 + \mathcal{O}(h^{4-2k}) + \mathcal{O}(\varepsilon) & \text{if } \bar{S} \text{ is smooth, } f \in \mathcal{C}^3, \\ \mathcal{O}(h^2) + \mathcal{O}(\varepsilon) & \text{if a discontinuity crosses } S. \end{cases}$$

*Proof.* Clearly, by definition and the fact that  $J, \tau \geq 0$ , there holds  $0 \leq \omega \leq 1$ .

Let us first assume that  $\bar{S}$  is smooth with  $k \in \{0, 1\}$ . Then, according to [3, Lemma 2], if  $k = 0$ ,  $I_{2,i} = \bar{\mathcal{O}}(h^2)$ ,  $i \in \{0, 1, 2\}$ , and if  $k = 1$ , then there exists  $i_0 \in \{0, 1, 2\}$  such that  $I_{2,i_0} = \bar{\mathcal{O}}(h^s)$ , for some  $s \in \{4, 5, 6, \dots\}$ , and  $I_{2,i} = \bar{\mathcal{O}}(h^4)$ , for  $i \in \{0, 1, 2\}$ ,  $i \neq i_0$ .

Therefore, combining this, we deduce that  $I_{2,0} + I_{2,1} = \bar{\mathcal{O}}(h^{2+2k})$  and that  $I_{2,1} + I_{2,2} = \bar{\mathcal{O}}(h^{2+2k})$ . Moreover, since either  $I_{2,0} = \bar{\mathcal{O}}(h^{2+2k})$  or  $I_{2,2} = \bar{\mathcal{O}}(h^{2+2k})$ , it can be concluded that

$$J = I_{2,0}(I_{2,1} + I_{2,2}) + (I_{2,0} + I_{2,1})I_{2,2} = \bar{\mathcal{O}}(h^{4+4k}) + \mathcal{O}(\varepsilon).$$

On the other hand,

$$\begin{aligned} d &= (-f_{-1} + 3f_0 - 3f_1 + f_2)^2 = \mathcal{O}(h^6) = \mathcal{O}(h^6) + \mathcal{O}(\varepsilon), \\ I &= I_0 + I_1 + I_2 = \mathcal{O}(h^{2+2k}) = \mathcal{O}(h^{2+2k}) + \mathcal{O}(\varepsilon). \end{aligned}$$

Therefore  $\tau = \mathcal{O}(h^{8+2k})$ . Hence, and since by assumption  $J \neq 0$ ,

$$\begin{aligned} \omega &= \frac{J}{J + \tau + \varepsilon} = \frac{1}{1 + \frac{\tau}{J}} - \mathcal{O}(\varepsilon) = \frac{1}{1 + \frac{\mathcal{O}(h^{8+2k})}{\bar{\mathcal{O}}(h^{4+4k})}} - \mathcal{O}(\varepsilon) = \frac{1}{1 + \mathcal{O}(h^{4-2k})} - \mathcal{O}(\varepsilon) \\ &= 1 - \mathcal{O}(h^{4-2k}) - \mathcal{O}(\varepsilon). \end{aligned}$$

Finally, let us assume that a discontinuity crosses  $S$ . Then there exists  $i_0 \in \{0, 1\}$ , such that  $I_{2,i_0} = \bar{\mathcal{O}}(1)$ . On the other hand,  $I_{2,|1-i_0|} = \bar{\mathcal{O}}(h^{2m_0})$  and  $I_{2,2} = \bar{\mathcal{O}}(h^{2m_1})$ , for some  $1 \leq m_0, m_1 \in \{1, 2, 3, \dots\}$ . Now, by these considerations, we have

$$I_{2,0}(I_{2,1} + I_{2,2}) = \begin{cases} \bar{\mathcal{O}}(h^m) & \text{if } i_0 = 0, \\ \bar{\mathcal{O}}(h^{m_0}) & \text{if } i_0 = 1, \end{cases} \quad (I_{2,0} + I_{2,1})I_{2,2} = \bar{\mathcal{O}}(h^{m_1})$$

with  $m := \max\{m_0, m_1\}$ .

Under any of these combinations, we obtain

$$J = I_{2,0}(I_{2,1} + I_{2,2}) + (I_{2,0} + I_{2,1})I_{2,2} = \bar{\mathcal{O}}(h^{2m}).$$

On the other hand, since in this case there holds

$$\begin{aligned} d &= (-f_{-1} + 3f_0 - 3f_1 + f_2)^2 = \bar{\mathcal{O}}(1) = \bar{\mathcal{O}}(1) + \mathcal{O}(\varepsilon), \\ I &= I_0 + I_1 + I_2 = \bar{\mathcal{O}}(1) = \bar{\mathcal{O}}(1) + \mathcal{O}(\varepsilon), \end{aligned}$$

then  $\tau = \bar{\mathcal{O}}(1)$  and

$$\begin{aligned} \omega &= \frac{J}{J + \tau + \varepsilon} = \frac{1}{1 + \frac{\tau}{J}} - \mathcal{O}(\varepsilon) = \frac{1}{1 + \frac{\bar{\mathcal{O}}(1)^2}{\bar{\mathcal{O}}(h^{2m})}} - \mathcal{O}(\varepsilon) = \frac{1}{1 + \frac{\bar{\mathcal{O}}(1)}{\bar{\mathcal{O}}(h^{2m})}} - \mathcal{O}(\varepsilon) \\ &= \frac{1}{1 + \bar{\mathcal{O}}(h^{-2m})} - \mathcal{O}(\varepsilon) = \frac{1}{\bar{\mathcal{O}}(h^{-2m})} - \mathcal{O}(\varepsilon) = \bar{\mathcal{O}}(h^{2m}) + \mathcal{O}(\varepsilon) = \mathcal{O}(h^2) + \mathcal{O}(\varepsilon), \end{aligned}$$

which completes the proof.  $\square$

Now, let us focus on the computation of the corrected weights.

PROPOSITION 3. *For  $i \in \{0, 1\}$ , there holds*

$$\omega_i = \begin{cases} c_i + \mathcal{O}(h^{4-2k}) + \mathcal{O}(\varepsilon) & \text{if } \bar{S} \text{ contains smooth data,} \\ \mathcal{O}(h^2) + \mathcal{O}(\varepsilon) & \text{if a discontinuity crosses } S_i, \\ \mathcal{O}(1) + \mathcal{O}(\varepsilon) & \text{if a discontinuity crosses } S, \text{ but not } S_i. \end{cases}$$

*Proof.* We first recall that  $\omega_i = \omega c_i + (1 - \omega)\tilde{\omega}_i$ . If  $\omega = 1 - \mathcal{O}(h^{m_0}) - \mathcal{O}(\varepsilon)$  for some  $m_0 \geq 0$ , then

$$\omega_i = (1 - \mathcal{O}(h^{m_0}) - \mathcal{O}(\varepsilon))c_i + (\mathcal{O}(h^{m_0}) + \mathcal{O}(\varepsilon))\tilde{\omega}_i = c_i + \mathcal{O}(h^{m_0}) + \mathcal{O}(\varepsilon),$$

where we have taken into account that  $\tilde{\omega}_i$  is an expression at most  $\mathcal{O}(1)$ , since in particular  $0 \leq \tilde{\omega}_i \leq 1$ . Therefore, using Proposition 2, we obtain the result.

On the other hand, if  $\omega$  satisfies  $\omega = \mathcal{O}(h^{2m_1}) + \mathcal{O}(\varepsilon)$  for some  $m_1 \geq 1$ , then

$$\omega_i = (\mathcal{O}(h^{2m_1}) + \mathcal{O}(\varepsilon))c_i + (1 - \mathcal{O}(h^{2m_1}) - \mathcal{O}(\varepsilon))\tilde{\omega}_i = \tilde{\omega}_i + \mathcal{O}(h^{2m_1}) + \mathcal{O}(\varepsilon).$$

Hence, in this case we must focus on the analysis of the accuracy for  $\omega_i$ . By Proposition 2 we have that  $\omega = \mathcal{O}(h^{2m_1})$ ,  $m_1 > 0$ , if a discontinuity crosses  $S$ .

In such case, there exists  $i_0 \in \{0, 1\}$  such that  $I_{i_0} = \bar{\mathcal{O}}(1)$ , whereas  $I_{1-i_0} = \mathcal{O}(h^2)$ . Therefore, in this case we have

$$\begin{aligned} \tilde{\omega}_{i_0} &= \frac{I_{1-i_0} + \varepsilon}{I_0 + I_1 + 2\varepsilon} = \frac{\mathcal{O}(h^2)}{\bar{\mathcal{O}}(1)} + \mathcal{O}(\varepsilon) = \mathcal{O}(h^2) + \mathcal{O}(\varepsilon), \\ \tilde{\omega}_{1-i_0} &= \frac{I_{i_0} + \varepsilon}{I_0 + I_1 + 2\varepsilon} = \frac{\bar{\mathcal{O}}(1)}{\bar{\mathcal{O}}(1)} + \mathcal{O}(\varepsilon) = \mathcal{O}(1) + \mathcal{O}(\varepsilon). \end{aligned}$$

Therefore, taking into account that  $\omega_i = \tilde{\omega}_i + \mathcal{O}(h^{2m_1}) + \mathcal{O}(\varepsilon)$  with  $m_1 \geq 1$ , we obtain

$$\omega_{i_0} = \mathcal{O}(h^2) + \mathcal{O}(\varepsilon), \quad \omega_{1-i_0} = \mathcal{O}(1) + \mathcal{O}(\varepsilon). \quad \square$$

THEOREM 4. *The reconstruction  $p(x_{1/2})$  satisfies*

$$p(x_{1/2}) = \begin{cases} f(x_{1/2}) + \mathcal{O}(h^3) & \text{if } \bar{S} \text{ is smooth,} \\ f(x_{1/2}) + \mathcal{O}(h^2) & \text{if a discontinuity crosses } S. \end{cases}$$

*Proof.* This is a direct consequence of the application of Proposition 3 to the expression (2.9), taking also into account that both for reconstructions from point values and from cell averages, the ideal weights  $c_i$ ,  $i \in \{0, 1\}$ , satisfy that  $c_0 p_0(x_{1/2}) + c_1 p_1(x_{1/2})$  equals the corresponding third-order reconstruction of the same type at  $x_{1/2}$ .  $\square$

REMARK 2.1. *The cases in which the order of the critical point is  $k \geq 2$  are not covered, since with this assumption any reconstruction, regardless of the degree of the corresponding polynomials, will attain an order of at least  $k + 1 \geq 3$ , and therefore the accuracy will be optimal regardless of the values of the weights  $\omega_i$ , taking into consideration that they always are a convex combination, namely,  $\omega_0, \omega_1 \geq 0$  and  $\omega_0 + \omega_1 = 1$ .*

**Summary of the algorithm.** Input:  $\bar{S} = \{f_{-1}, f_0, f_1, f_2\}$ , with  $f_i = f(x_i)$  or  $f_i = \frac{1}{h} \int_{x_{i-1/2}}^{x_{i+1/2}} f(x) dx$ , and  $\varepsilon > 0$ .

1. Compute the corresponding interpolating polynomials evaluated at  $x_{1/2}$ , which, both in case of reconstructions from point values and from cell averages, are given by (2.2).
2. Compute the corresponding Jiang-Shu smoothness indicators  $I_0, I_1$  and  $I_2$  (including the one considering the rightmost node) by (2.1) and (2.4).
3. Compute the preliminary weights  $\tilde{\omega}_0$  and  $\tilde{\omega}_1$  from (2.5).
4. Define  $\tau$  by (2.7).
5. Compute the corrector weight  $\omega$  from (2.6).
6. Compute the corrected weights  $\omega_0$  and  $\omega_1$  from (2.8).
7. Obtain the OWENO reconstruction at  $x_{1/2}$ :

$$p_2(x_{1/2}) = \omega_0 p_0(x_{1/2}) + \omega_1 p_1(x_{1/2}).$$

Output:  $\mathcal{R}(f_{-1}, f_0, f_1, f_2, \varepsilon) := p_2(x_{1/2})$ .

**3. WENO schemes for systems of conservation laws.** In this section, we discuss the incorporation of the novel third-order WENO approach in the context of hyperbolic conservation laws. The purpose is to prove that the resulting scheme has the same computational domain as a standard third-order WENO reconstruction based on a three-point stencil.

**3.1. Hyperbolic systems of conservation laws.** We will briefly describe in this section the equations and their discretization procedure. We consider hyperbolic systems of  $\nu$  scalar conservation laws in  $d$  space dimensions:

$$(3.1) \quad \mathbf{u}_t + \sum_{i=1}^d \mathbf{f}^i(\mathbf{u})_{x_i} = \mathbf{0}, \quad (\mathbf{x}, t) \in \Omega \times \mathbb{R}^+ \subseteq \mathbb{R}^d \times \mathbb{R}^+, \quad \mathbf{x} = (x_1, \dots, x_d),$$

where  $\mathbf{u} = \mathbf{u}(\mathbf{x}, t) \in \mathbb{R}^\nu$  is the sought solution,  $\mathbf{f}^i : \mathbb{R}^\nu \rightarrow \mathbb{R}^\nu$  are given flux density vectors, and

$$\mathbf{u} = \begin{pmatrix} u_1 \\ \vdots \\ u_\nu \end{pmatrix}, \quad \mathbf{f}^i = \begin{pmatrix} f_1^i \\ \vdots \\ f_\nu^i \end{pmatrix}, \quad i = 1, \dots, d; \quad \mathbf{f} = [\mathbf{f}^1 \quad \dots \quad \mathbf{f}^d].$$

System (3.1) is complemented with the initial condition

$$u(\mathbf{x}, 0) = \mathbf{u}_0(\mathbf{x}), \quad \mathbf{x} \in \Omega,$$

and prescribed boundary conditions.

To describe the spatial discretization, we introduce a Cartesian grid  $\mathcal{G}$  formed by points (cell centers)  $\mathbf{x} = \mathbf{x}_{j_1, \dots, j_d} = ((j_1 - \frac{1}{2})h, \dots, (j_d - \frac{1}{2})h) \in \mathcal{G}$  for  $h > 0$ . In what follows, we use the index vector  $\mathbf{j} = (j_1, \dots, j_d)$ , let  $\mathbf{e}_i$  denote the  $i$ -th  $d$ -dimensional unit vector, and assume that  $J$  is the set of all indices  $\mathbf{j}$  for which point values of the solution are to be computed. We then advance a semi-discrete scheme in which spatial derivatives are discretized first, resulting in a system of ordinary differential equations whose numerical solution is iteratively updated in time. To do so, we first define

$$\mathbf{U}(t) := (\mathbf{u}(\mathbf{x}_j, t))_{j \in J}.$$

To solve (3.1) we utilize the Shu-Osher finite difference scheme [17, 18] with upwind spatial reconstructions of the flux function that are incorporated into numerical flux vectors  $\hat{\mathbf{f}}^i$  through a Donat-Marquina flux-splitting [5]. Thus, the contribution to the flux divergence in the coordinate  $x_i$  at point  $\mathbf{x} = \mathbf{x}_j$  is given by

$$\mathbf{f}^i(\mathbf{U})_{x_i}(\mathbf{x}_j, t) \approx \frac{1}{h} \left( \hat{\mathbf{f}}_{j+\frac{1}{2}\mathbf{e}_i}^i(\mathbf{U}(t)) - \hat{\mathbf{f}}_{j-\frac{1}{2}\mathbf{e}_i}^i(\mathbf{U}(t)) \right).$$

Then, WENO reconstructions [9] of order  $2r+1$  are considered, with special emphasis on the case we are interested in, namely,  $r = 1$  (order 3). To specify the time discretization, we write the semi-discrete scheme compactly as

$$\frac{d}{dt} \mathbf{U}(t) = \mathcal{L}(\mathbf{U}(t)), \quad \mathcal{L}(\mathbf{U}(t)) = (\mathcal{L}_j(\mathbf{U}(t)))_{j \in J},$$

where we define

$$\mathcal{L}_j(\mathbf{U}(t)) := \frac{1}{h} \sum_{i=1}^d \left( \hat{\mathbf{f}}_{j+\frac{1}{2}\mathbf{e}_i}^i(\mathbf{U}(t)) - \hat{\mathbf{f}}_{j-\frac{1}{2}\mathbf{e}_i}^i(\mathbf{U}(t)) \right)$$

(with suitable modifications for boundary points).

For the time discretization, we either use the third-order Runge-Kutta TVD scheme proposed in [18] or the approximate Lax-Wendroff (henceforth, LWA) approach proposed in [24], which in turn is based on the original Lax-Wendroff (henceforth, LW) approach proposed by Qiu and Shu in [13]. This will be specified in each numerical experiment.

**3.2. Third-order WENO scheme.** Although it may seem that the overall scheme for finite dimensional conservation laws uses more points than the corresponding scheme for classical WENO3 reconstructions, it is not the case, as we now show.

The semidiscrete scheme for a scalar one-dimensional law is

$$(3.2) \quad u_i'(t) = -\frac{1}{h} (\hat{f}_{i+1/2} - \hat{f}_{i-1/2}),$$

$$(3.3) \quad \hat{f}_{i+1/2} = \hat{f}(u_{i-1}, u_i, u_{i+1}, u_{i+2}),$$

so that the the right-hand side of (3.2) depends on approximations  $u_j(t) \approx u(x_j, t)$  at a 5-point stencil  $j = i - 2, \dots, i + 2$ . An ODE solver, as the TVD Runge-Kutta 3 proposed in [18], is applied to (3.2) to obtain the final time-space accurate scheme.

If the reconstruction (3.3) associated with the cell interface  $x_{i+1/2}$  is sought and we define the interval  $I(a, b) := [\min\{a, b\}, \max\{a, b\}]$ , then we determine for  $j \in$

$\{i-1, i, i+1, i+1\}$  the quantities

$$f_j^{i+1/2,+} := \begin{cases} f(u_j) & \text{if } f'(u) > 0 \text{ for all } u \in I(u_i, u_{i+1}), \\ 0 & \text{if } f'(u) < 0 \text{ for all } u \in I(u_i, u_{i+1}), \\ f(u_j) + \alpha_{i+1/2} u_j & \text{otherwise,} \end{cases}$$

$$f_j^{i+1/2,-} := \begin{cases} 0 & \text{if } f'(u) > 0 \text{ for all } u \in I(u_i, u_{i+1}), \\ f(u_j) & \text{if } f'(u) < 0 \text{ for all } u \in I(u_i, u_{i+1}), \\ f(u_j) - \alpha_{i+1/2} u_j & \text{otherwise,} \end{cases}$$

where

$$\alpha_{i+1/2} := \max_{u \in I(u_i, u_{i+1})} |f'(u)|.$$

The precise formulation (see [18]) for attaining third-order accuracy (the maximum for semidiscrete stability being three for this 5-point stencil, cf. [2] for the usual WENO3 reconstructions) consists in using a local flux splitting  $f(u) = f^+(u) + f^-(u)$ , such that  $\pm(f^\pm(u))' \geq 0$ , in the interval  $I(u_i, u_{i+1}]$  determined by  $u_i$  and  $u_{i+1}$ , which is defined as

$$(3.4) \quad \hat{f}_{i+1/2} := \mathcal{R}^+(f_{i-1}^{i+1/2,+}, f_i^{i+1/2,+}, f_{i+1}^{i+1/2,+}) \\ + \mathcal{R}^-(f_i^{i+1/2,-}, f_{i+1}^{i+1/2,-}, f_{i+2}^{i+1/2,-}),$$

where  $\mathcal{R}^+$  is a right-biased cell-averages reconstruction and is the right-biased cell-averages reconstruction given by  $\mathcal{R}^-(a, b, c) = \mathcal{R}^+(c, b, a)$ .

In contrast, the flux splitting and reconstruction used herein are defined as follows. Instead of using (3.4), we propose to define the flux value  $\hat{f}_{i+1/2}$  by our optimal-order reconstruction  $\mathcal{R}^{\pm, \text{opt}}$  that depends on the four-point stencil, such that

$$\hat{f}_{i+1/2} = \hat{f}(u_{i-1}, u_i, u_{i+1}, u_{i+2}) \\ = \mathcal{R}^{+, \text{opt}}(f_{i-1}^{i+1/2,+}, f_i^{i+1/2,+}, f_{i+1}^{i+1/2,+}, f_{i+2}^{i+1/2,+}) \\ + \mathcal{R}^{-, \text{opt}}(f_{i-1}^{i+1/2,-}, f_i^{i+1/2,-}, f_{i+1}^{i+1/2,+}, f_{i+2}^{i+1/2,-}).$$

Systems of conservation laws are dealt with the application of the former scheme to local characteristic fields, obtained with a double linearization [5]. The extension to multidimensional Cartesian grids is straightforwardly obtained by working dimension by dimension.

## 4. Numerical experiments.

**4.1. Accuracy tests with algebraic problems.** We perform some tests in order to verify the accuracy properties of the scheme in presence of critical points. In order to perform these experiments, we will use the multiple-precision library MPFR [12] through its C++ wrapper [8], using a precision of 3322 bits ( $\approx 1000$  digits) and taking in all the cases  $\varepsilon = 10^{-10^6}$ .

Let us consider the family of functions  $f_k : \mathbb{R} \rightarrow \mathbb{R}$ ,  $k \in \{0, 1\}$ , given by  $f_k(x) = x^{k+1}e^x$ . Then  $f_k$  has a smooth extremum at  $x = 0$  of order  $k$ . In this case the error is given by  $E_{k,n} = |P_n(0) - f_k(0)|$ , with  $P_n$  the corresponding reconstruction at  $x_{1/2} = 0$ , with the grid  $x_i = (i-1/2)h$ ,  $i \in \{-1, \dots, 1+s\}$  ( $s = 0$  for the traditional JS-WENO and YC-WENO schemes and  $s = 1$  for the proposed optimal WENO schemes, in

	$\theta$	$k$	JSWENO3		YCWENO3		OWENO3	
			Point	Cell	Point	Cell	Point	Cell
$f_k$	—	0	3.00	3.00	2.98	2.98	3.00	3.00
	—	1	2.00	2.00	2.00	2.00	<b>3.01</b>	<b>3.01</b>
$g_k$	0	0	1.97	1.93	1.98	1.98	2.00	2.00
	0	1	1.99	1.99	1.99	1.99	1.96	1.95
	1	0	2.00	2.00	2.00	2.00	1.99	2.00
	1	1	2.00	2.00	2.00	2.00	2.00	2.00

TABLE 1  
Numerical order for third-order schemes, functions with smooth extrema.

which an additional node is considered), with  $h = 1/n$  for  $n \in \mathbb{N}$ , when pointwise values are taken, namely,  $f_{k,i} = f_k(x_i)$  and reconstructions from pointwise values to pointwise values are performed. On the other hand, we also present in the tables the same setup when cell average values are taken instead:

$$f_{k,i} = \int_{x_i-h/2}^{x_i+h/2} f(x) dx,$$

by performing reconstructions from cell average values to pointwise values. In all the cases, the tables show the corresponding average orders,  $O_k = \frac{1}{80} \sum_{j=1}^{80} o_{k,j}$ , where  $o_{k,j} = \log_2(E_{k,n_{j-1}}/E_{k,n_j})$ , with  $n_j = 5 \cdot 2^j$ ,  $j \in \{0, \dots, 80\}$ .

We also consider alternatively the family of functions  $g_k : \mathbb{R} \rightarrow \mathbb{R}$ ,  $k \in \{0, 1\}$  given by

$$g_k(x) = \begin{cases} x^{2k} e^x & \text{for } x \leq 0, \\ e^{x+1} & \text{for } x > 0. \end{cases}$$

Then  $g_k$  has a discontinuity at  $x = 0$  with a left smooth extremum of order  $k$  for  $k \in \{0, 1\}$ . We test the accuracy of the methods with the same parameters as above, where, in order to emphasize the behaviour of our optimal scheme at discontinuities, in this case we change the location of the discontinuity by considering a grid of the form  $x_i = (i - \frac{1}{2} + \theta)h$ ,  $i \in \{-1, \dots, 1 + s\}$ , for  $\theta \in \{0, 1\}$ . Since  $x_{1/2} = \theta h$ , the error in this case is thus given by  $|P(\theta h) - g(\theta h)|$ .

The results involving the different combinations of the proposed values for  $k$  in the case of  $f_k$  and for  $\theta$  and  $k$  in the case of  $g_k$  are shown in Table 1 for the traditional JSWENO3 and YC-WENO3 schemes as well as the optimal WENO approach presented herein.

We discuss row by row the results obtained in Table 1. The first two rows containing data stand for the function  $f_k$ , which is a smooth function with a critical point of order  $k$ . Therefore, the optimal order is 3. We can see that when the critical point has order zero, namely,  $k = 0$ , all the schemes attain the optimal accuracy. However, differences arise when  $k = 1$ . In this case, the first order critical point affects the traditional WENO schemes decreasing its accuracy in one unit, whereas the optimal WENO approach keeps the optimal third order accuracy.

As for the function  $g_k$ , we can conclude that regardless of the position of the discontinuity with respect to the stencil  $S$  and the order of the critical point, all the schemes, both the traditional ones and the optimal ones, attain the suboptimal second-order accuracy, avoiding the error of magnitude  $\mathcal{O}(1)$  associated to the substencil

$n$	JSWENO3				YCWENO3				OWENO3			
	$\ \cdot\ _1$		$\ \cdot\ _\infty$		$\ \cdot\ _1$		$\ \cdot\ _\infty$		$\ \cdot\ _1$		$\ \cdot\ _\infty$	
	Err.	$\mathcal{O}$	Err.	$\mathcal{O}$	Err.	$\mathcal{O}$	Err.	$\mathcal{O}$	Err.	$\mathcal{O}$	Err.	$\mathcal{O}$
40	8.52e-03	—	2.56e-02	—	6.67e-03	—	2.11e-02	—	1.87e-04	—	3.08e-04	—
80	2.10e-03	2.02	1.00e-02	1.36	1.46e-03	2.19	7.90e-03	1.42	2.31e-05	3.02	3.66e-05	3.07
160	4.86e-04	2.11	3.81e-03	1.39	3.19e-04	2.20	2.87e-03	1.46	2.86e-06	3.01	4.50e-06	3.02
320	1.10e-04	2.15	1.43e-03	1.42	6.45e-05	2.31	1.02e-03	1.50	3.56e-07	3.01	5.60e-07	3.01
640	2.45e-05	2.16	5.28e-04	1.43	1.32e-05	2.29	3.54e-04	1.52	4.44e-08	3.00	6.98e-08	3.00
1280	5.42e-06	2.18	1.94e-04	1.45	2.61e-06	2.34	1.21e-04	1.55	5.55e-09	3.00	8.72e-09	3.00
2560	1.19e-06	2.19	7.06e-05	1.46	5.05e-07	2.37	4.10e-05	1.56	6.93e-10	3.00	1.09e-09	3.00
5120	2.57e-07	2.21	2.56e-05	1.46	9.69e-08	2.38	1.37e-05	1.58	8.67e-11	3.00	1.36e-10	3.00
10240	5.54e-08	2.21	9.22e-06	1.47	1.84e-08	2.40	4.53e-06	1.60	1.08e-11	3.00	1.71e-11	2.99
20480	1.19e-08	2.22	3.31e-06	1.48	3.44e-09	2.42	1.49e-06	1.61	1.43e-12	2.92	2.38e-12	2.84

TABLE 2

Example 1: linear advection equation, third-order schemes.

containing the discontinuity. This is the best order of accuracy that can be obtained near a discontinuity by shock-capturing methods based on three- or four-point stencils.

**4.2. Conservation laws experiments.** In this section we present some experiments involving numerical solutions of hyperbolic conservation laws. In order to discretize them in time, we will use the approximate Lax-Wendroff approach matching the spatial order proposed in [24], unless we indicate the contrary, in whose case the RK3-TVD schemes will be used. Also, since in this case we work with double precision, the  $\varepsilon$  parameter is chosen as  $\varepsilon = 10^{-100}$ . The flux splitting used is Donat-Marquina [5] for the problems with weak solutions and LLF for the problems with smooth solutions (unless all the characteristics move to the same direction, in whose case we simply use the corresponding left/right-biased upwind reconstructions). In all cases, and also unless we state the contrary, the CFL used for the 1D experiments is 0.5 and for the 2D experiments 0.4.

**Example 1: Linear advection equation.** We consider the linear advection equation with the following domain, boundary condition and initial condition:

$$u_t + f(u)_x = 0, \quad \Omega = (-1, 1), \quad u(-1, t) = u(1, t),$$

$$f(u) = u, \quad u_0(x) = 0.25 + 0.5 \sin(\pi x),$$

whose exact solution is  $u(x, t) = 0.25 + 0.5 \sin(\pi(x - t))$ , with critical points located at  $x = t + m + 1/2$ ,  $m \in \mathbb{Z}$ .

We run several simulations with final time  $T = 1$ , resolutions of  $n$  points, that is, with a grid spacing of  $h = 2/n$ , using the classical JS-WENO schemes, YC-WENO and our OWENO3 scheme, both with the  $\|\cdot\|_1$  and  $\|\cdot\|_\infty$  errors. Since the characteristics move to the right, we use right-biased reconstructions. The results are shown in Table 2. From the table it can be clearly appreciated that an accuracy loss is produced in the case of the traditional schemes, whereas the optimal third-order accuracy is solidly kept by the optimal third-order scheme.

**Examples 2a and 2b: Burgers equation.** We now consider Burgers equation with the following setup involving the domain, boundary conditions and initial condition:

$$(4.1) \quad u_t + f(u)_x = 0, \quad \Omega = (-1, 1), \quad u(-1, t) = u(1, t),$$

$$f(u) = u^2/2, \quad u_0(x) = 0.25 + 0.5 \sin(\pi x).$$

$n$	JSWENO3				YCWENO3				OWENO3			
	$\ \cdot\ _1$		$\ \cdot\ _\infty$		$\ \cdot\ _1$		$\ \cdot\ _\infty$		$\ \cdot\ _1$		$\ \cdot\ _\infty$	
	Err.	$\mathcal{O}$	Err.	$\mathcal{O}$	Err.	$\mathcal{O}$	Err.	$\mathcal{O}$	Err.	$\mathcal{O}$	Err.	$\mathcal{O}$
40	1.77e-03	—	1.11e-02	—	1.62e-03	—	9.85e-03	—	1.70e-04	—	1.11e-03	—
80	4.77e-04	1.89	4.17e-03	1.41	4.21e-04	1.95	3.57e-03	1.46	2.24e-05	2.92	1.81e-04	2.62
160	1.18e-04	2.02	1.62e-03	1.36	9.80e-05	2.10	1.32e-03	1.43	2.75e-06	3.03	2.27e-05	3.00
320	2.91e-05	2.02	6.21e-04	1.38	2.24e-05	2.13	4.94e-04	1.42	3.37e-07	3.03	2.77e-06	3.03
640	7.01e-06	2.06	2.36e-04	1.40	5.05e-06	2.15	1.79e-04	1.46	4.16e-08	3.02	3.41e-07	3.02
1280	1.64e-06	2.10	8.84e-05	1.42	1.11e-06	2.18	6.36e-05	1.50	5.17e-09	3.01	4.23e-08	3.01
2560	3.83e-07	2.10	3.28e-05	1.43	2.47e-07	2.17	2.21e-05	1.52	6.44e-10	3.00	5.26e-09	3.01
5120	8.85e-08	2.11	1.20e-05	1.45	5.45e-08	2.18	8.84e-06	1.32	8.04e-11	3.00	6.56e-10	3.00
10240	2.04e-08	2.11	5.42e-06	1.15	1.21e-08	2.17	4.41e-06	1.00	1.00e-11	3.00	8.19e-11	3.00
20480	4.70e-09	2.12	2.73e-06	0.99	2.71e-09	2.16	2.21e-06	1.00	1.25e-12	3.00	1.02e-11	3.00

TABLE 3  
Example 2a: Burgers equation, third-order schemes.

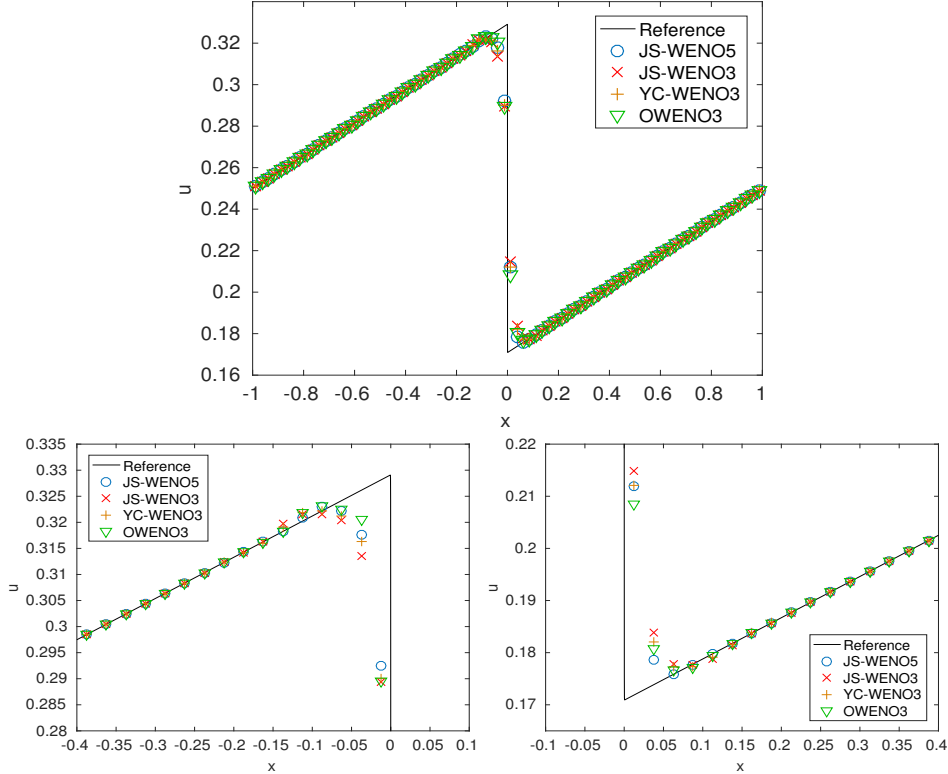


FIGURE 1. Example 2b (Burgers equation, discontinuous solution at  $T = 12$ ): third-order schemes.

In this case,  $f(u_0(x))$  has a first-order smooth extremum at  $x = -1/2$  and  $x = 1/2$ . In Example 2a, we consider the solution of (4.1) at  $T = 0.3$ , when it is still smooth, whose results are shown in Table 3, while in Example 2b we set  $T = 12$ , when the solution of (4.1) has become discontinuous, shown in Figure 1, in which are also compared against the results obtained by the widely used JS-WENO5 schemes.

From the tables one can see that again, as in the linear advection case, the presence of first-order critical points makes the accuracy of the traditional schemes decay to orders lower than three, while the third-order accuracy is still kept by the optimal

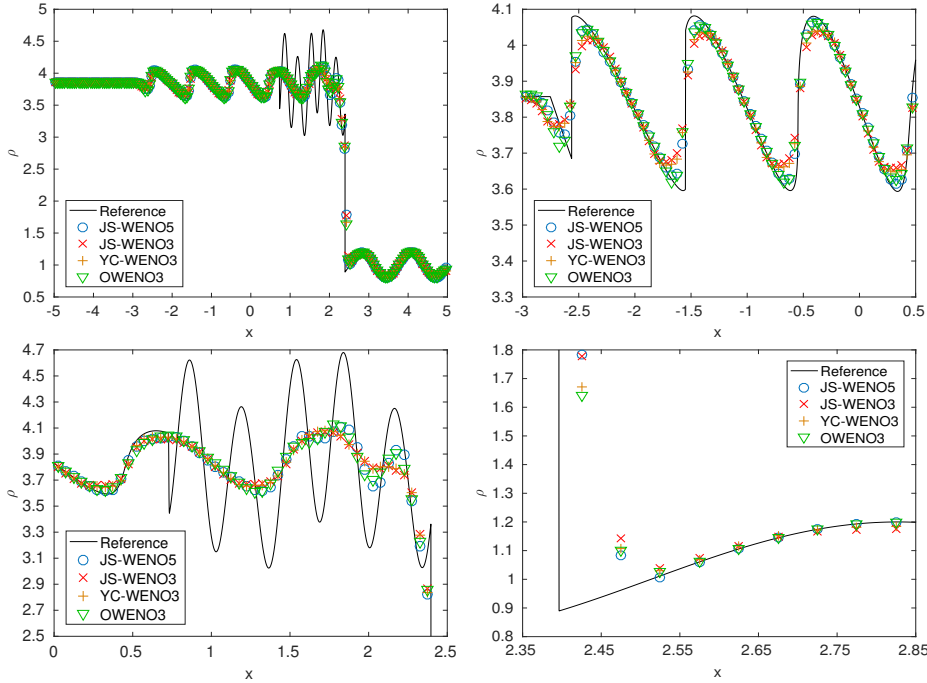


FIGURE 2. *Example 3a: Shu-Osher problem.  $T = 1.8$ .  $n = 200$ .*

third-order scheme. As for the discontinuous case, we can see that the optimal third-order scheme has a much higher resolution than the traditional third-order schemes, especially near the discontinuity and, moreover, it is similar than the resolution presented by the fifth-order scheme.

**Examples 3a and 3b: Shu-Osher problem.** The 1D Euler equations for gas dynamics are given by  $\mathbf{u} = (\rho, \rho v, E)^T$  and  $\mathbf{f}(\mathbf{u}) = \mathbf{f}^1(\mathbf{u}) = (\rho v, p + \rho v^2, v(E + p))^T$ , where  $\rho$  is the density,  $v$  is the velocity and  $E$  is the specific energy of the system. The variable  $p$  stands for the pressure and is given by the equation of state  $p = (\gamma - 1)(E - \rho v^2/2)$ , where  $\gamma$  is the adiabatic constant that will be taken as  $\gamma = 1.4$ . We now consider the interaction with a Mach 3 shock and a sine wave. The spatial domain is now given by  $\Omega := (-5, 5)$  with the initial condition

$$(\rho, v, p)(x, 0) = \begin{cases} (27/7, 4\sqrt{35}/9, 31/3) & \text{if } x \leq -4, \\ (1 + \sin(5x)/5, 0, 1) & \text{if } x > -4, \end{cases}$$

with left inflow and right outflow boundary conditions.

We run the simulation until  $T = 1.8$  and compare the schemes against a reference solution computed with a resolution of  $n = 16000$  cells. Figures 2 and 3 are associated to the third-order schemes and JS-WENO5 with resolutions of  $n = 200$  and  $n = 400$  points, respectively, showing the corresponding density fields.

As it can be seen, the third-order optimal schemes show again a much better resolution than their traditional counterparts, especially observed in the resolution of  $n = 400$  cells. Moreover, they have a similar resolution than the JS-WENO5 scheme, and at lower computational cost.

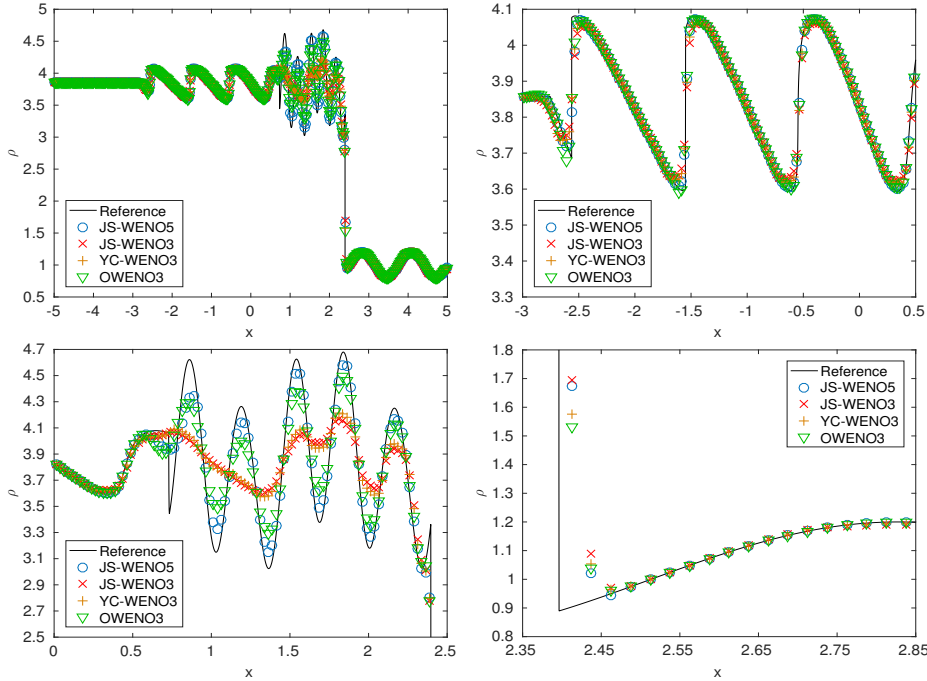


FIGURE 3. *Example 3a: Shu-Osher problem.  $T = 1.8$ .  $n = 400$ .*

In order to verify the latter statement, we next present an efficiency comparison involving the ratio error  $\|\cdot\|_1 / \text{CPU time}$ , which can be seen in Figure 4.

We can see that in this case all the proposed optimal third-order scheme shows a much better performance than its traditional counterparts. Moreover, it is also more efficient than the JS-WENO5 scheme as the figure shows.

**Examples 4a and 4b: Blast wave problem.** Continuing with the 1D Euler equations, let us now simulate the interaction of two blast waves [4] by using the following initial data

$$u(x, 0) = \begin{cases} u_L & 0 < x < 0.1, \\ u_M & 0.1 < x < 0.9, \\ u_R & 0.9 < x < 1, \end{cases}$$

where  $\rho_L = \rho_M = \rho_R = 1$ ,  $v_L = v_M = v_R = 0$ ,  $p_L = 10^3$ ,  $p_M = 10^{-2}$ ,  $p_R = 10^2$ . We set reflecting boundary conditions at  $x = 0$  and  $x = 1$ , simulating a solid wall at both sides. This problem involves multiple reflections of shocks and rarefactions off the walls and many interactions of waves inside the domain.

The results are shown in Figure 5 for the density field at a resolution of  $n = 800$  cells, in which all the third-order schemes involved in this paper are used, being in turn compared with the JS-WENO5 scheme. The resolution used for the reference solution is  $n = 100000$  cells.

As the results show, the third-order optimal scheme has at some regions a higher resolution than even the fifth-order scheme.

Finally, Figure 6 shows an efficiency comparison between all the involved schemes, where, for the sake of performing a fair comparison, all the schemes have been equipped with a RK3-TVD scheme. In this case, the optimal third-order scheme

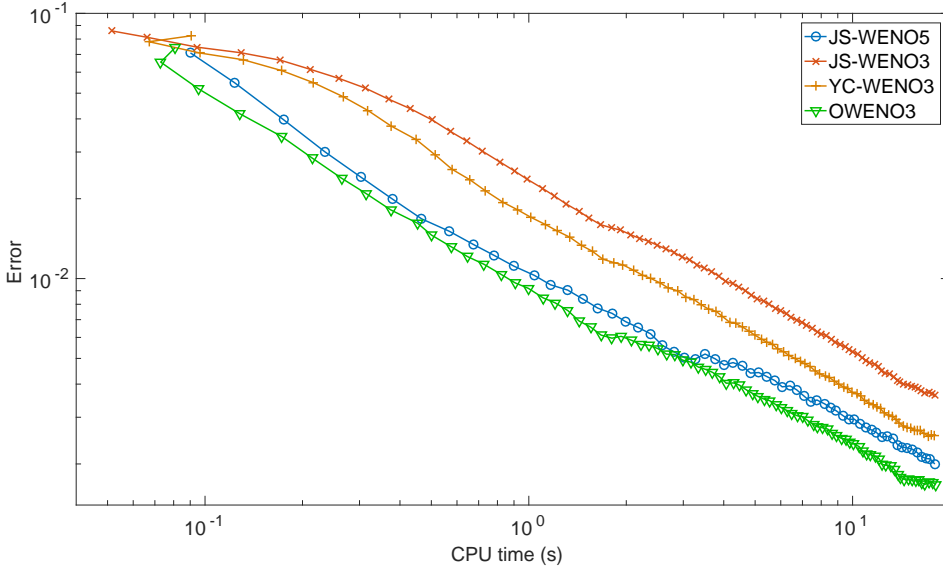


FIGURE 4. Example 3b: Ratio Error/CPU comparison for Shu-Osher problem.

is still more efficient than the fifth-order scheme.

**Examples 5a and 5b: Double Mach reflection.** The equations that will be considered in this section are the two-dimensional Euler equations for inviscid gas dynamics given by

$$(4.2) \quad \mathbf{u}_t + \sum_{i=1}^d \mathbf{f}^i(\mathbf{u})_{x_i} = \mathbf{0}, \quad (\mathbf{x}, t) \in \Omega \times \mathbb{R}^+ \subseteq \mathbb{R}^d \times \mathbb{R}^+, \quad \mathbf{x} = (x_1, \dots, x_d),$$

by taking in (4.2)  $m = 4$  and  $d = 2$ , where setting  $x = x_1$  and  $y = x_2$ , we have

$$\mathbf{u} = \begin{pmatrix} \rho \\ \rho v^x \\ \rho v^y \\ E \end{pmatrix}, \quad \mathbf{f}^1(\mathbf{u}) = \begin{pmatrix} \rho v^x \\ p + \rho(v^x)^2 \\ \rho v^x v^y \\ v^x(E + p) \end{pmatrix}, \quad \mathbf{f}^2(\mathbf{u}) = \begin{pmatrix} \rho v^y \\ \rho v^x v^y \\ p + \rho(v^y)^2 \\ v^y(E + p) \end{pmatrix}.$$

Here  $\rho$  is the density,  $(v^x, v^y)$  is the velocity,  $E$  is the specific energy, and  $p$  is the pressure that is given by the equation of state  $p = (\gamma - 1)(E - \rho((v^x)^2 + (v^y)^2)/2)$ , where the adiabatic constant is again chosen as  $\gamma = 1.4$ .

This experiment uses these equations to model a vertical right-going Mach 10 shock colliding with an equilateral triangle. By symmetry, this is equivalent to a collision with a ramp with a slope of  $30^\circ$  with respect to the horizontal line.

For the sake of simplicity, in [4] it is considered the equivalent problem in a rectangle, consisting in a rotated shock, whose vertical angle is  $30^\circ$ . The domain is the rectangle  $\Omega = [0, 4] \times [0, 1]$ , and the initial conditions are

$$(\rho, v^x, v^y, E)(x, y, 0) = \begin{cases} \mathbf{c}_1 = (\rho_1, v_1^x, v_1^y, E_1) & \text{if } y \leq \frac{1}{4} + \tan(\frac{\pi}{6})x, \\ \mathbf{c}_2 = (\rho_2, v_2^x, v_2^y, E_2) & \text{if } \frac{1}{4} + \tan(\frac{\pi}{6})x, \end{cases}$$

$$\mathbf{c}_1 = (8, 8.25 \cos(\pi/6), -8.25 \sin(\pi/6), 563.5), \quad \mathbf{c}_2 = (1.4, 0, 0, 2.5).$$

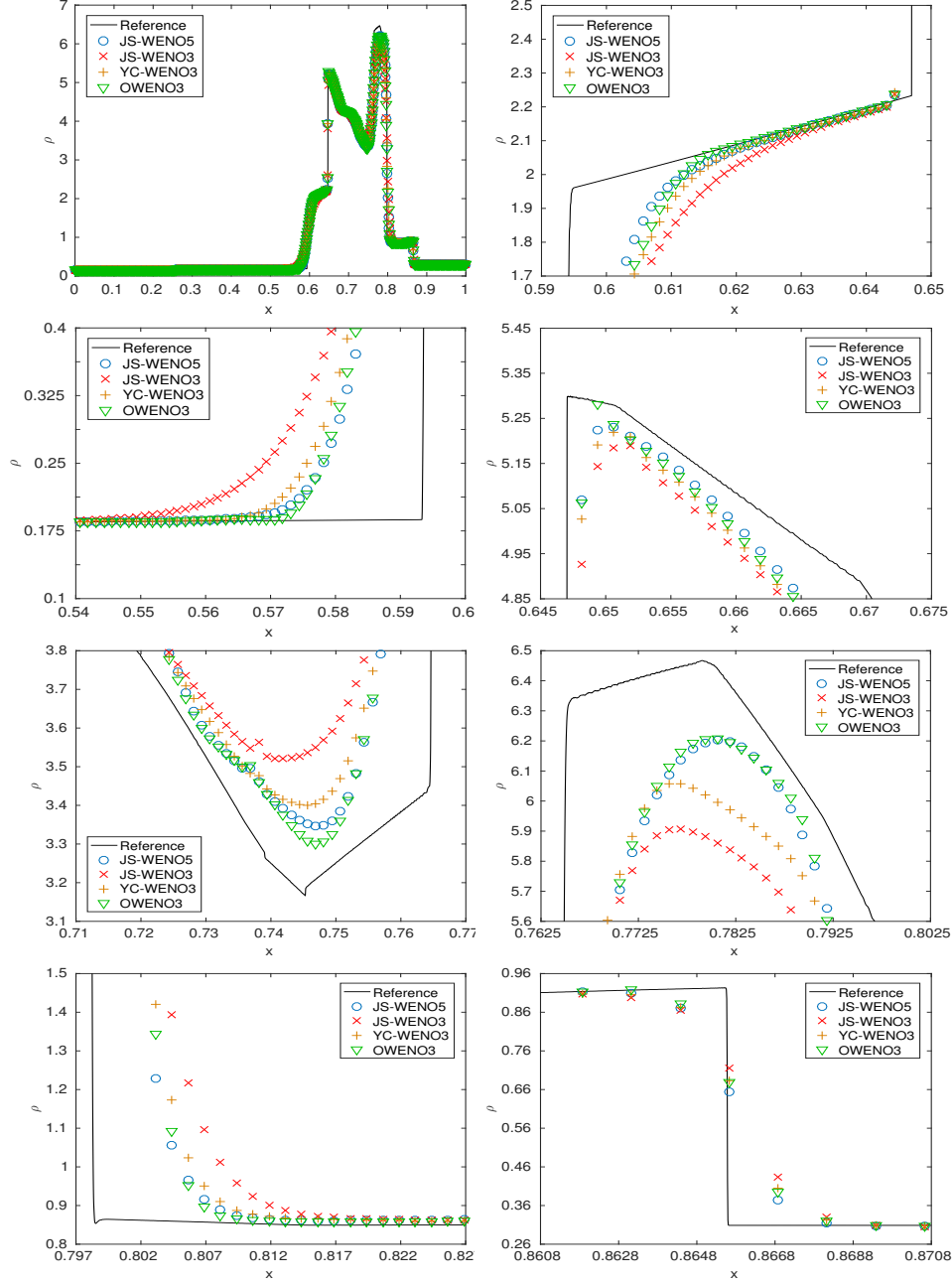


FIGURE 5. Example 4a: Blast wave problem.  $T = 0.038$ .

We impose inflow boundary conditions, with value  $c_1$ , at the left side,  $\{0\} \times [0, 1]$ , outflow boundary conditions both at  $[0, \frac{1}{4}] \times \{0\}$  and  $\{4\} \times [0, 1]$ , reflecting boundary conditions at  $[\frac{1}{4}, 4] \times \{0\}$  and inflow boundary conditions at the upper side,  $[0, 4] \times \{1\}$ ,

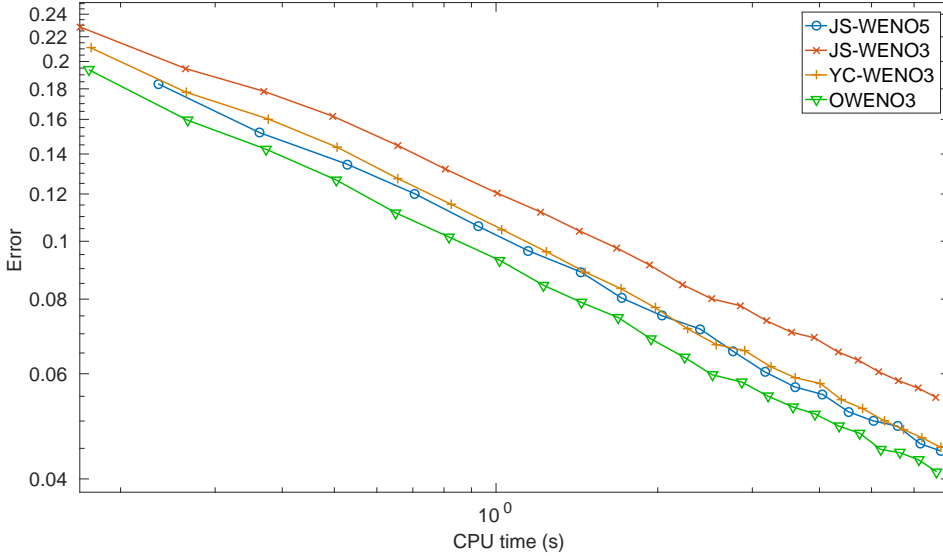


FIGURE 6. *Example 4b: Ratio Error/CPU comparison for blast wave problem.*

which mimics the shock at its actual traveling speed:

$$(\rho, v^x, v^y, E)(x, 1, t) = \begin{cases} \mathbf{c}_1 & \text{if } x \leq \frac{1}{4} + \frac{1+20t}{\sqrt{3}}, \\ \mathbf{c}_2 & \text{if } x > \frac{1}{4} + \frac{1+20t}{\sqrt{3}}. \end{cases}$$

We run different simulations until  $T = 0.2$  at a resolution of  $2560 \times 640$  points, shown in Figure 7, with  $\text{CFL} = 0.4$  and involving the classical JS-WENO5 scheme and the third-order schemes considered along this paper.

In this case, we can see that in both resolutions, both the YC-WENO3 scheme and the OWENO3 scheme have a higher resolution than the JS-WENO3 scheme, in which the discontinuities and the non-smooth features such as turbulence and vorticity are more smeared. On the other hand, the resolution shown by the former schemes is still remarkably lower than the JS-WENO5 scheme. This is probably due to the nature of this problem, which has no solution for the inviscid 2D Euler equations, since more and more turbulences and vorticities appear at smaller levels as resolution is increased.

Indeed, it is well known that the resolution obtained in this particular problem is strongly related with the number of points used for the reconstructions, so that, unlike the other problems presented herein, in this case increasing arbitrarily the order of the scheme seems to improve considerably its efficiency.

Finally, in order to stress out the performance of our schemes, with the different time discretizations, at a same resolution, we show in Table 4 the computational time taken by all these combinations.

One can see that, for instance, the typically used JS-WENO5 schemes combined with a RK3-TVD time discretization is almost three times slower than any of the third-order optimal WENO approaches with an approximate Lax-Wendroff time discretization.

**Examples 6a and 6b: 2D Riemann problem.** Finally, we solve numerically a Riemann problem for the 2D Euler equations on the domain  $(0, 1) \times (0, 1)$ . Riemann

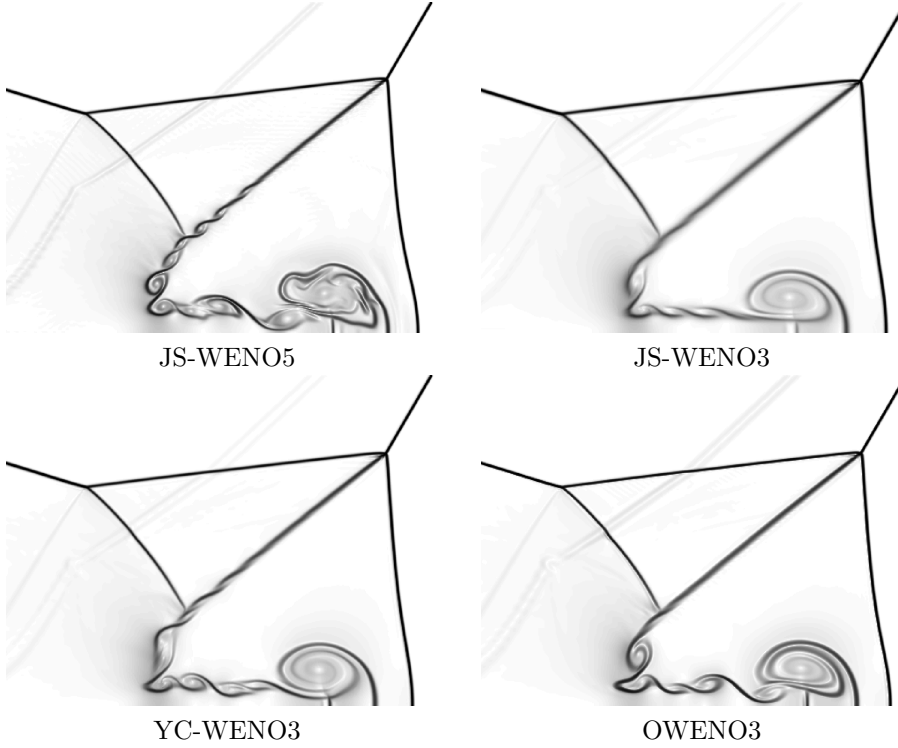


FIGURE 7. *Example 5a: Double Mach reflection, 2560 × 640. T = 0.2.*

	RK3	LW	ALW
JS-WENO5	85.76	65.63	64.53
JS-WENO3	56.56	33.72	30.46
YC-WENO3	57.04	34.42	30.82
OWENO3	58.83	35.23	31.48

TABLE 4

*Example 5b: computational time (seconds) with a resolution of 256 × 64 grid points. T = 0.2, CFL = 0.25.*

problems for 2D Euler equations were first studied in [16]. The initial data is taken from [10, Sect. 3, Config. 3]:

$$\mathbf{u}(x, y, 0) = (\rho(x, y, 0), \rho(x, y, 0)v^x(x, y, 0), \rho(x, y, 0)v^y(x, y, 0), E(x, y, 0))$$

and

$$\begin{pmatrix} \rho(x, y, 0) \\ v^x(x, y, 0) \\ v^y(x, y, 0) \\ p(x, y, 0) \end{pmatrix}^T = \begin{cases} (1.5, 0, 0, 1.5) & \text{for } x > 0.5, y > 0.5, \\ (0.5323, 1.206, 0, 0.3) & \text{for } x \leq 0.5, y > 0.5, \\ (0.138, 1.206, 1.206, 0.029) & \text{for } x \leq 0.5, y \leq 0.5, \\ (0.5323, 0, 1.206, 0.3) & \text{for } x > 0.5, y \leq 0.5, \end{cases}$$

with the same equation of state as in the previous test.

We impose outflow boundary conditions everywhere and run this test up to time  $T = 0.3$ . The results can be observed in Figure 8 for a resolution of 2560 × 2560 points.

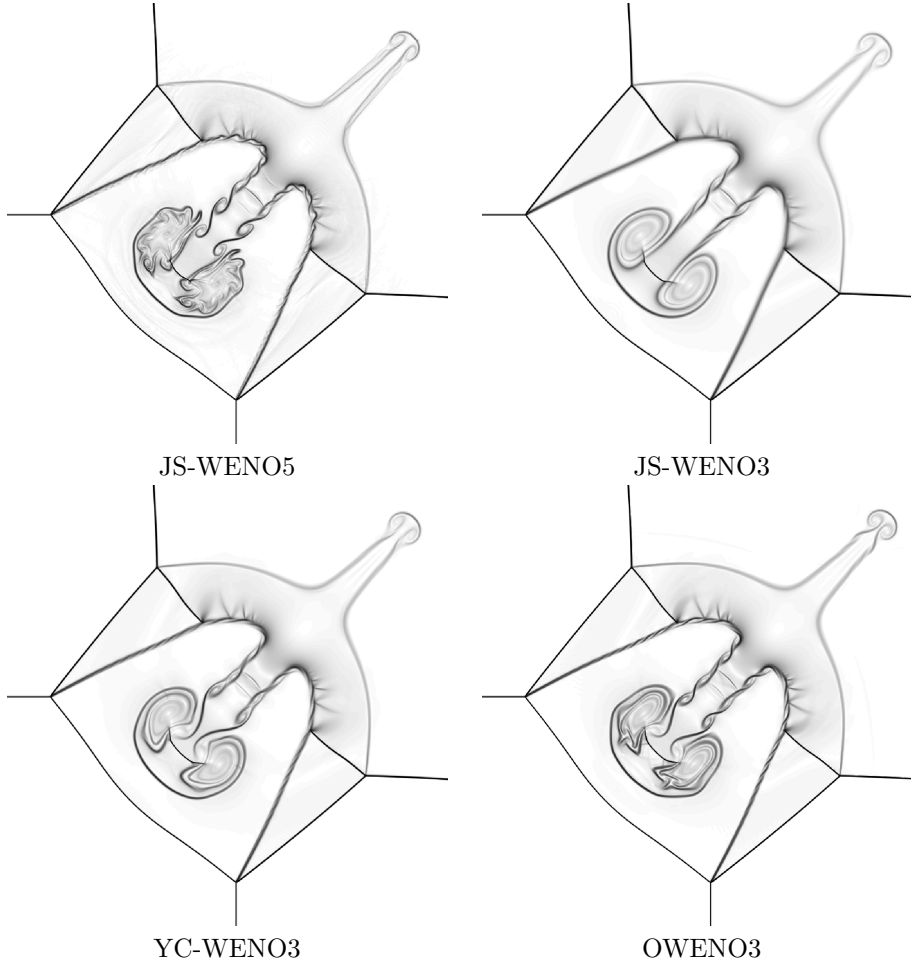


FIGURE 8. *Example 6a: 2D Riemann problem,  $2560 \times 2560$ .  $T = 0.3$ .*

From the results, it can be seen that the order from lower to higher resolution is again the following one: JS-WENO3, YC-WENO3, OWENO3 and JS-WENO5, being the two latter ones close to reach other. This is very significant if one takes into account that OWENO3 is faster than JS-WENO5.

With the purpose of analyzing more accurately the efficiency associated to each scheme, we now use the solutions computed with the grid of  $2560 \times 2560$  points as reference solutions to perform efficiency tests by comparing error versus CPU time involving numerical solutions with grid sizes  $16 \cdot 2^n \times 16 \cdot 2^n$ ,  $n \in \{0, 1, 2, 3, 4\}$ , for the involved schemes. The results are shown in Figure 9 and again indicate a higher performance for the OWENO3 scheme with respect to their third-order traditional counterparts.

**5. Conclusions.** In this paper a third-order scheme based on a weighted essentially non-oscillatory approach with unconditionally third-order optimal accuracy on smooth data has been presented. The accuracy properties have been proved theoretically and confirmed numerically along experiments involving static algebraic problems and hyperbolic conservation laws. This scheme has been proven in most of the ex-

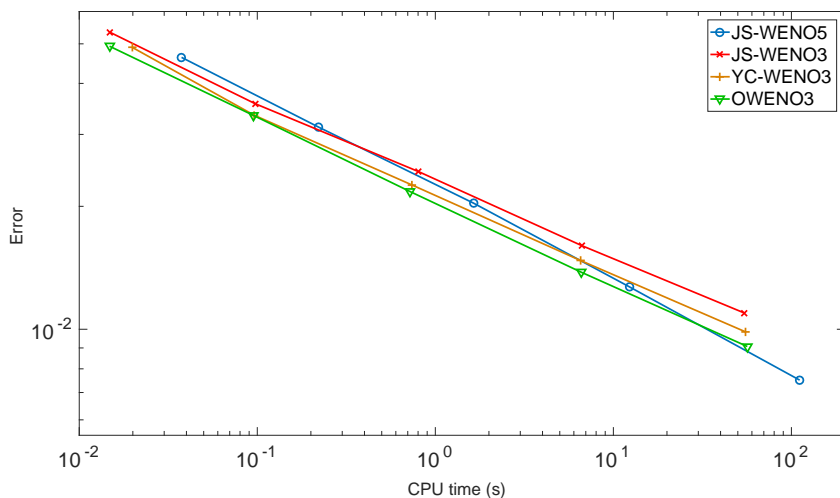


FIGURE 9. Example 6b: 2D Riemann problem, efficiency plot.

periments shown to be more efficient than even the classical fifth-order JS-WENO scheme widely used in the literature. Only in some problems involving very small-scale features, like the double Mach reflection test, the fifth-order method seems worth applying.

**Acknowledgements.** AB, PM and DZ are supported by Spanish MINECO projects MTM2017-83942-P. RB is supported by Fondecyt project 1170473; CONICYT/PIA/Concurso Apoyo a Centros Científicos y Tecnológicos de Excelencia con Financiamiento Basal AFB170001; CRHIAM, project CONICYT/FONDAP/15130015, and by the INRIA Associated Team “Efficient numerical schemes for non-local transport phenomena” (NOLOCO; 2018–2020). PM is also supported by Conicyt (Chile), project PAI-MEC, folio 80150006. DZ is also supported by Conicyt (Chile) through Fondecyt project 3170077.

## REFERENCES

- [1] F. ARÀNDIGA, A. BAEZA, A.M. BELDA, AND P. MULET, *Analysis of WENO schemes for full and global accuracy*, SIAM J. Numer. Anal., 49 (2011), pp. 893–915.
- [2] A. BAEZA, P. MULET AND D. ZORÍO, *The maximal order of semidiscrete schemes for quasilinear first order partial differential equations*, arXiv:1607.00210, (2016).
- [3] A. BAEZA, R. BÜRGER, P. MULET, AND D. ZORÍO, *On the efficient computation of smoothness indicators for a class of WENO reconstructions*, J. Sci. Comput., to appear.
- [4] P. WOODWARD AND P. COLELLA, *The numerical simulation of two-dimensional fluid flow with strong shocks*, J. Comput. Phys., 54 (1984), pp. 115–173.
- [5] R. DONAT AND A. MARQUINA, *Capturing shock reflections: An improved flux formula*, J. Comput. Phys., 125 (1996), pp. 42–58.
- [6] N.R. GANDE, Y. RATHOD AND S. RATHAN, *Third-order WENO scheme with a new smoothness indicator*, Int. J. Numer. Meth. Fluids, 85 (2017), pp. 90–112.
- [7] N.R. GANDE, Y. RATHOD AND S. RATHAN, *Improved third-order weighted essentially nonoscillatory scheme*, Int. J. Numer. Meth. Fluids, 87 (2018), pp. 329–342.
- [8] P. HOLOBORODKO, *MPFR C++*, <http://www.holoborodko.com/pavel/mpfr/>
- [9] G.S. JIANG AND C.-W. SHU, *Efficient implementation of Weighted ENO schemes*, J. Comput. Phys., 126 (1996), pp. 202–228.
- [10] A. KURGANOV AND E. TADMOR, *Solution of two-dimensional Riemann problems for gas dynamics without Riemann problem solvers*, Numer. Methods Partial Differential Equations,

- 18 (2002), pp. 584–608.
- [11] X.-D. LIU, S. OSHER, AND T. CHAN, *Weighted essentially non-oscillatory schemes*, J. Comput. Phys., 115 (1994), pp. 200–212.
  - [12] *The GNU MPFR library*, <http://www.mpfr.org/>
  - [13] J. QIU AND C.-W. SHU, *Finite difference WENO schemes with Lax-Wendroff-type time discretizations*, J. Sci. Comput., 24(6) (2003), pp. 2185–2198.
  - [14] B. SCHMIDTMANN, R. ABGRALL, AND M. TORRILHON, *On third-order limiter functions for finite volume methods*, Bull. Braz. Math. Soc. (N. S.), 47 (2016), pp. 753–764.
  - [15] B. SCHMIDTMANN, R. ABGRALL, AND M. TORRILHON, *Relations between WENO3 and third-order limiting in finite volume methods*, J. Sci. Comput., 68 (2016), pp. 624–652.
  - [16] C.W. SCHULZ-RINNE, *Classification of the Riemann problem for two-dimensional gas dynamics*, SIAM J. Math. Anal., 24 (1993), pp. 76–88.
  - [17] C.-W. SHU AND S. OSHER, *Efficient implementation of essentially non-oscillatory shock-capturing schemes*, J. Comput. Phys., 77 (1988), pp. 439–471.
  - [18] C.-W. SHU AND S. OSHER, *Efficient implementation of essentially non-oscillatory shock-capturing schemes, II*, J. Comput. Phys., 83 (1989), pp. 32–78.
  - [19] X. WU, J. LIANG, Y. ZHAO, *A new smoothness indicator for third-order WENO scheme*, Int. J. Numer. Meth. Fluids, 81 (2017), pp. 451–459.
  - [20] X. WU, Y. ZHAO, *A high-resolution hybrid scheme for hyperbolic conservation laws*, Int. J. Numer. Meth. Fluids, 78 (2015), pp. 162–187.
  - [21] W. XU AND W. WU, *An improved third-order weighted essentially non-oscillatory scheme achieving optimal order near critical points*, Computers and Fluids, 162 (2018), pp. 113–125.
  - [22] N.K. YAMALEEV AND M.H. CARPENTER, *Third-order energy stable WENO scheme*, J. Comput. Phys., 228 (2009), pp. 3025–3047.
  - [23] N.K. YAMALEEV AND M.H. CARPENTER, *A systematic methodology to for constructing high-order energy stable WENO schemes*, J. Comput. Phys., 228 (2009), pp. 4248–4272.
  - [24] D. ZORÍO, A. BAEZA, AND P. MULET, *An approximate Lax-Wendroff-type procedure for high-order accurate schemes for hyperbolic conservation laws*, J. Sci. Comput., 71 (2017), pp. 246–273.

# Centro de Investigación en Ingeniería Matemática (CI<sup>2</sup>MA)

## PRE-PUBLICACIONES 2019

- 2019-08 MANUEL SOLANO, FELIPE VARGAS: *An unfitted HDG method for Oseen equations*
- 2019-09 RAIMUND BÜRGER, STEFAN DIEHL, MARÍA CARMEN MARTÍ: *A system of conservation laws with discontinuous flux modelling flotation with sedimentation*
- 2019-10 ANDREA CANGIANI, MAURICIO MUNAR: *A posteriori error estimates for mixed virtual element methods*
- 2019-11 ALFREDO BERMÚDEZ, BIBIANA LÓPEZ-RODRÍGUEZ, RODOLFO RODRÍGUEZ, PILAR SALGADO: *Numerical analysis of a penalty approach for the solution of a transient eddy current problem*
- 2019-12 JAVIER A. ALMONACID, GABRIEL N. GATICA, RICARDO RUIZ-BAIER: *Ultra-weak symmetry of stress for augmented mixed finite element formulations in continuum mechanics*
- 2019-13 MARIO ÁLVAREZ, GABRIEL N. GATICA, RICARDO RUIZ-BAIER: *A mixed-primal finite element method for the coupling of Brinkman-Darcy flow and nonlinear transport*
- 2019-14 MARCELO CAVALCANTI, WELLINGTON CORREA, TÜRKER ÖZSARI, MAURICIO SEPÚLVEDA, RODRIGO VÉJAR: *Exponential stability for the nonlinear Schrödinger equation with locally distributed damping*
- 2019-15 RICARDO OYARZÚA, MANUEL SOLANO, PAULO ZUÑIGA: *A priori and a posteriori error analyses of a high order unfitted mixed-FEM for Stokes flow*
- 2019-16 DAVID MORA, IVÁN VELÁSQUEZ: *Virtual element for the buckling problem of Kirchhoff-Love plates*
- 2019-17 VERONICA ANAYA, BRYAN GOMEZ-VARGAS, DAVID MORA, RICARDO RUIZ-BAIER: *Incorporating variable viscosity in vorticity-based formulations for Brinkman equations*
- 2019-18 FELIPE LEPE, DAVID MORA: *Symmetric and non-symmetric discontinuous Galerkin methods for a pseudostress formulation of the Stokes spectral problem*
- 2019-19 ANTONIO BAEZA, RAIMUND BÜRGER, PEP MULET, DAVID ZORÍO: *An efficient third-order WENO scheme with unconditionally optimal accuracy*

Para obtener copias de las Pre-Publicaciones, escribir o llamar a: DIRECTOR, CENTRO DE INVESTIGACIÓN EN INGENIERÍA MATEMÁTICA, UNIVERSIDAD DE CONCEPCIÓN, CASILLA 160-C, CONCEPCIÓN, CHILE, TEL.: 41-2661324, o bien, visitar la página web del centro: <http://www.ci2ma.udec.cl>



**CENTRO DE INVESTIGACIÓN EN  
INGENIERÍA MATEMÁTICA (CI<sup>2</sup>MA)  
Universidad de Concepción**



Casilla 160-C, Concepción, Chile  
Tel.: 56-41-2661324/2661554/2661316  
<http://www.ci2ma.udec.cl>

